DALTON
FULL PAPER

# A pyracylene model for the interaction of transition metals with fullerenes: a density functional study

**Francesca Nunzi,[a] Antonio Sgamellotti *[a] and Nazzareno Re [b]**

[a] *Dipartimento di Chimica e Centro Studi CNR per il Calcolo Intensivo in Scienze Molecolari, Università di Perugia, I-06123 Perugia, Italy. E-mail: sgam@thch.unipg.it*
[b] *Facoltà di Farmacia, Università G. D'Annunzio, I-66100 Chieti, Italy*

***Received 2nd February 2001, Accepted 7th November 2001***
***First published as an Advance Article on the web 10th January 2002***

Pyracylene, a polynuclear aromatic hydrocarbon which is made up of two benzene and two cyclopentadienyl rings, has been employed as a model to study the interaction of transition metal complexes with fullerenes. To reproduce adequately the geometric and electronic structure of fullerene with a pyracylene model, we had to impose suitable geometric constraints forcing the pyramidalisation angle on the two central carbon atoms to assume a value similar to that observed in $C_{60}$. Density functional calculations were then performed on $(PH_3)_2M(C_{14}H_8)$ (M = Ni, Pd, Pt) molecules. The results have been analysed in terms of the Chatt–Dewar–Duncanson model and show that the constrained pyracylene is a fairly good model to study the interaction of transition metals with fullerene: geometries are reproduced within 0.02 Å and the bond dissociation energies are slightly underestimated by only 10–40 kJ $mol^{-1}$.

## 1 Introduction

The increasing interest recently attracted by fullerenes has led to a growing attention to polynuclear aromatic hydrocarbons (PAHs) that may be considered as substructures of the $C_{60}$ surface.[1–4] The simplest of these fullerene fragments that exhibits a curved structure is corannulene, $C_{20}H_{10}$, which has a central five-membered ring surrounded by five hexagonal rings.[5] However the smallest carbon framework that can be identified on the buckminsterfullerene surface is pyracylene, $C_{14}H_8$, which is made up by the fusion of two benzene and two cyclopentadienyl rings (see Fig. 1). Although free pyracylene is a planar molecule and thus lacks the characteristic curved structure of fullerenes, it has long been proposed as a model for studying the reactivity of $C_{60}$.[6,7]

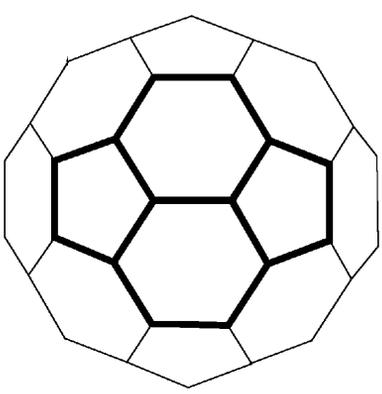

**Fig. 1** Pyracylene's structure superposed on the $C_{60}$ surface.

In this report we use pyracylene as a model to study the interaction of transition metal complexes with fullerenes. In the fullerene cage we can distinguish two kinds of bonds, corresponding to the fusion of two six-membered rings, [6,6] bond, and of a six-membered and a five-membered ring, [6,5] bond. The electron density is mainly localised on the [6,6] bond and the metal atom is attached in a di-hapto fashion to a [6,6] bond in the transition metal complexes. The fullerene molecule has been considered as composed of six pyramidalised pyracylene units fused octahedrally, each unit showing one [6,6] and four [6,5] bonds, see Fig. 1. Metal attachment causes a distortion of the geometry and a variation of the electronic structure of the $C_{60}$ moiety restricted to the pyracylene unit directly bonded to the metal fragment, while negligible deviations (within 0.03 Å with respect to free $C_{60}$) are observed in the other pyracylene units. It is therefore natural to use a pyracylene molecule to reproduce the metal–fullerene interaction. Accurate theoretical calculations on transition metal fullerene complexes have been limited by the large size of these species and only recently have geometry optimisations at correlated levels been performed.[8] In a recent paper, we reported an accurate theoretical study on the $(PH_3)_2M(\eta^2\text{-}C_{60})$ complexes for the Group 10 metals Ni, Pd and Pt at a DFT non-local level.[8] The electronic structure was analysed in terms of the Chatt–Dewar–Duncanson model and the contribution from $\pi$ back-donation was found to dominate over that from $\sigma$ donation for all three complexes. Reliable values for the metal fullerene bond dissociation energies were calculated.

In this paper we evaluate the reliability of the pyracylene model to reproduce the metal–fullerene interaction by comparing the geometries, the electronic structures and the bonding energies of $(PH_3)_2M(\eta^2\text{-}C_{14}H_8)$ (M = Ni, Pd, Pt) complexes with those of the corresponding fullerene complexes.

## 2 Computational details

The calculations reported in this paper are based on the ADF (Amsterdam Density Functional) program package.[9] Its main characteristics are the use of a density fitting procedure to obtain accurate Coulomb and exchange potentials in each SCF cycle, the accurate and efficient numerical integration of the effective one-electron Hamiltonian matrix elements and the possibility to freeze core orbitals. The molecular orbitals were expanded using a Slater-type orbital (STO) basis set. We performed our calculations on pyracylene complexes using two different basis sets. The first set, hereafter referred to as set I, consists of a double-$\zeta$ STO basis set for C (2s, 2p), P (3s, 3p), and H (1s) atoms, while a double-$\zeta$ STO basis set for *n*s and *n*p and a triple-$\zeta$ STO basis set for *n*d and $(n + 1)$s has been used for the transition metal atoms ($n = 3$, 4, 5 respectively for Ni, Pd,

DOI: 10.1039/b101145f

Pt). As polarisation functions, we used one ($n$ + 1)p function for transition metals, one 3d for P and C, and one 2p for H. The second basis set, hereafter called set II, differs from set I for the use of a triple-$\zeta$ STO basis set for C, P, and H. The frozen cores were 1s for C, 1s–2p for P, 1s–3p for Ni, 1s–3d for Pd and 1s–4d for Pt.

The LDA exchange correlation potential and energy were used, together with the Vosko–Wilk–Nusair parametrisation [10] for homogeneous electron gas correlation, including the Becke's non-local correction [11] to the local exchange expression and the Perdew's non-local correction [12] to the local expression of correlation energy.

Since the relativistic effects play an important role in describing the electronic structure and relative energetics of the species containing heavy metals, such as platinum, they were taken into account by the Pauli formalism, the Pauli Hamiltonian including first order scalar relativistic corrections (Darwin and mass–velocity) while neglecting spin–orbit corrections.[13,14]

Molecular structures of all considered complexes were optimised at this non-local (NL) level in $C_{2v}$ symmetry.

## 3 Results and discussion

### Geometry optimisation

We first performed a geometry optimisation on the pyracylene molecule $C_{14}H_8$ under $D_{2h}$ symmetry constraints. The results are reported in Table 1, where the values calculated with basis set II have been reported in parentheses. When comparing pyracylene parameters with those of fullerene, we refer to basis set I which has been employed in the latter calculations.[8] The C–C bond distances show a good agreement with the X-ray structure,[15,16] the deviations being within only 0.01 Å. As shown in Table 1, the C–C bonds pattern of pyracylene is quite different from that of $C_{60}$. In particular, the [6,6] bond distance in $C_{14}H_8$ (1.351 Å) is closer to a double C–C bond typical of ethylene (1.332 Å, evaluated at the same level of theory) rather than to a [6,6] bond in $C_{60}$ (1.392 Å). This is not surprising, because the C–C bond lengths in fullerenes are intrinsically connected to the curvature of the carbon surface.[7]

Borden and co-workers have investigated several strained olefins and their stabilisation upon formation of metal complexes.[17] Morokuma and Borden have reported *ab initio* calculations on $(PH_3)_2PtC_2H_4$ finding that an increase of pyramidalisation angle leads to an increase of the metal–ligand interaction.[18a] The same results have been obtained by Uddin *et al.* through DFT calculations on $Pt(PH_3)_2$ complexes of a series of highly pyramidalised tricyclic alkenes.[18b]

In order to reproduce adequately the geometric and electronic structure of fullerene with the pyracylene molecule, we imposed on this model a suitable geometric constraint, forcing the pyramidalisation angle on the two carbon atoms of the [6,6] bond to assume a value similar to that observed in $C_{60}$ ($\delta$ = 31.7°). This was achieved by freezing the cartesian coordinates of the hydrogen atoms of pyracylene along the direction of the C–C bonds, bracketing the pyracylene subunit in $C_{60}$ with a fixed C–H bond distance of 1.10 Å, the same value observed in free pyracylene. A geometry optimisation was then performed under this constraint, and the final structure shows a pyramidalisation angle of the two carbon atoms ($\delta$ = 37.0°) close to that of fullerene ($\delta$ = 31.7°).

The imposed distortion from planarity determines a lengthening of the C–C bonds: the [6,6] bond increases from 1.351 Å in the planar system to 1.419 Å in the out-of-plane structure, which is very close to the value calculated for $C_{60}$ at the same level of theory (1.392 Å), while the [5,6] bond lengthens from 1.402 Å to 1.444 Å, also very close to the value of 1.447 Å calculated for $C_{60}$. These geometrical parameters thus suggest that the bent $C_{14}H_8$ is a good model for $C_{60}$. As expected, this bending process has a high energetic cost, 289 kJ mol$^{-1}$. This energy difference between the planar and the bent pyracylene system is probably due to a partial loss of aromaticity.

**Table 1** Optimised geometries of fullerene's models compared to $C_{60}$. Bond lengths in angstroms and bond angles in degrees. Values calculated with basis set II are shown in parentheses

| Molecule | $\delta$ | $R_{[5,6]}$ | $R_{[6,6]}$ |
|---|---|---|---|
| $C_{14}H_8$ | 0 | 1.402 (1.408) | 1.351 (1.358) |
| $C_{14}H_8$ | 37.0 | 1.444 (1.447) | 1.419 (1.422) |
| $C_{14}H_8$ (R–X)[a] | 0 | 1.397 | 1.360 |
| $C_{60}$[b] | 31.7 | 1.447 | 1.392 |

[a] Refs. 15 and 16. [b] Ref. 8.

We then considered the complexes formed by this bent constrained pyracylene with $M(PH_3)_2$ metal fragments of the Ni, Pd, Pt triad. Geometry optimisations have been carried out on all of these $(PH_3)_2M(\eta^2\text{-}C_{14}H_8)$ complexes using both basis sets I and II. The results obtained are given in Table 2, where the values calculated with basis set II are reported in parentheses. When comparing pyracylene complex geometries with those of fullerene, we refer to basis set I, which has been employed in the latter calculations.[8]

All X-ray structures available for metal diphosphine fullerene complexes show the [6,6] C–C bond in the $MP_2$ plane rather than perpendicular to it, analogous to the situation observed for the corresponding ethylene complexes. All geometry optimisations on pyracylene complexes were therefore performed in the parallel orientation, setting the metal fragment on the [6,6] bond and imposing $C_{2v}$ symmetry constraints (see Fig. 2).

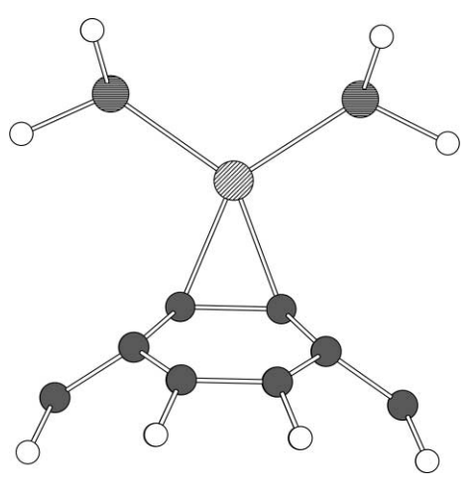

**Fig. 2** Geometry of $(PH_3)_2M(\eta^2\text{-}C_{14}H_8)$ complexes.

Analogously to fullerene complexes, the metal attachment causes a significant distortion in the pyracylene moiety, with a lengthening of the [6,6] bond and an increase of the pyramidalisation angle. Indeed the lengthening of the [6,6] C–C bond in the pyracylene unit is 0.05–0.08 Å, quite close to the value of 0.07–0.11 Å calculated using the whole fullerene unit. The metal coordination has the effect of pulling out two of the carbon atoms on the [6,6] bond from the average plane of the other carbon atoms, similar to that observed for $C_{60}$ complexes. The degree of pull-out is measured by the increase of the pyramidalisation angle in the metal complex with respect to the value observed for the free fragment. The degree of pull-out calculated for the pyracylene complexes, 4–6°, is quite similar to the value of 7–10° found for fullerene complexes. Also the M–C bond distances calculated for pyracylene complexes differ by less than 0.02 Å from that for fullerene complexes.

In order to estimate the effect of the geometrical constraints on the metal–pyracylene bond, we carried out a geometry optimisation also on the $(PH_3)_2Ni(\eta^2\text{-}C_{14}H_8)$ complex without

**Table 2** Optimised geometries of $(PH_3)_2M(C_{14}H_8)$ and $(PH_3)_2M(C_{60})$ complexes. Bond lengths in angstroms and bond angles in degrees. Values calculated with basis set II are shown in parentheses

| Molecule | $R_{([5,6])}$ | $R_{([6,6])}$ | $R_{(M-C)}$ | $R_{(M-P)}$ | ∠PMP | $\delta$ |
|---|---|---|---|---|---|---|
| $(PH_3)_2Ni(C_{14}H_8)$ | 1.461 | 1.483 | 2.012 | 2.208 | 112.1 | 42.2 |
| | (1.465) | (1.482) | (2.018) | (2.212) | (146.1) | (42.0) |
| $(PH_3)_2Pd(C_{14}H_8)$ | 1.451 | 1.465 | 2.170 | 2.393 | 125.3 | 40.6 |
| | (1.454) | (1.459) | (2.195) | (2.382) | (126.5) | (40.1) |
| $(PH_3)_2Pt(C_{14}H_8)$ | 1.464 | 1.503 | 2.112 | 2.277 | 117.3 | 42.9 |
| | (1.469) | (1.528) | (2.065) | (2.271) | (116.0) | (44.4) |
| $(PH_3)_2Ni(C_{60})$ | 1.474 | 1.470 | 1.989 | 2.222 | 113.0 | 39.3 |
| $(PH_3)_2Pd(C_{60})$ | 1.471 | 1.464 | 2.180 | 2.378 | 111.0 | 38.8 |
| $(PH_3)_2Pt(C_{60})$ | 1.485 | 1.505 | 2.103 | 2.289 | 107.4 | 41.8 |
| $(PH_3)_2Ni(C_{14}H_8)$ | 1.435 | 1.401 | 2.071 | 2.181 | 115.1 | 27.6 |
| Planar | (1.439) | (1.405) | (2.085) | (2.189) | (114.3) | (26.7) |

any constraints on the organic moiety. We found a longer M–C bond distance (0.07 Å) and a shorter C–C bond distance (0.08 Å) with respect to the corresponding constrained pyracylene complex. The pyramidalisation angle is 27°, a value markedly lower than the one calculated for the nickel fullerene complex.[8] These results indicate that the constrained bending of pyracylene is essential to reproduce the geometrical features of fullerene metal complexes.

## Bonding energies

The bond dissociation energies between the $C_{14}H_8$ and $M(PH_3)_2$ fragments, $D(M–C_{14}H_8)$, have been calculated according to the following scheme:

$$(PH_3)_2M(\eta^2\text{-}C_{14}H_8) \longrightarrow M(PH_3)_2 + C_{14}H_8 \qquad (1)$$

where both the pyracylene complex and the two fragments have been considered in their ground-state equilibrium geometries. As for fullerene complexes, we calculated the above bond dissociation energies in two steps (see Scheme 1). We first evaluated

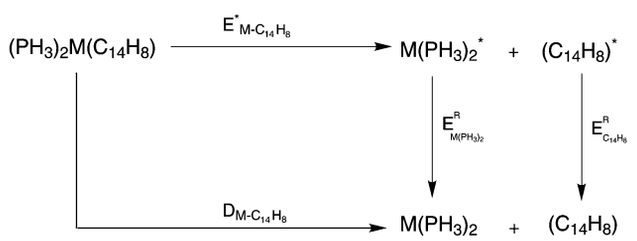


**Scheme 1**

the "snapping energies", $E^*(M–C_{14}H_8)$, *i.e.* the energy required to snap the metal–ligand bond into non-reorganised fragments, and then we computed the energies $E^R_{C_{14}H_8}$ and $E^R_{M(PH_3)_2}$, *i.e.* the relaxation energies of the two fragments. We also calculated the basis set superposition error (BSSE), by applying the counterpoise method.[19] Corrections for zero-point vibration were not included since they are expected to give small contributions.

The results obtained are given in Table 3, and are compared to the values calculated in ref. 8. The metal–pyracylene bond dissociation energy increases in the order Pd < Pt < Ni. Such an order for metal–ligand bond strength within the nickel triad could be surprising considering the order observed from geometrical distortion of pyracylene complexes (*i.e.* Pd < Ni < Pt). Indeed, the optimised geometries in Table 2 indicate clearly a higher degree of distortion of the coordinated pyracylene in the platinum than in the nickel complex, thus suggesting a reversed bond strength order, *i.e.* Ni < Pt. This dichotomy has been already observed for olefins[20] and fullerene complexes,[8] and rationalised on the basis of the relaxation energies of the metal fragments. The same rationale applies here: the order of the metal–pyracylene bond dissociation energies for Pt and Ni, 64 (109) and 123 (117) kJ $mol^{-1}$ respectively (see Table 3), are determined by the large reorganisation energy of the $Pt(PH_3)_2$ fragment, −104 (−126) kJ $mol^{-1}$, with respect to −42 (−42) kJ $mol^{-1}$ for $Ni(PH_3)_2$, while the order of the bond energy terms is reversed, 183 (251) and 173 (168) kJ $mol^{-1}$, respectively for Pt and Ni.

The comparison between the calculated parameters for pyracylene and fullerene complexes (see Table 3) shows that the bond dissociation energies of pyracylene complexes are smaller than those of the corresponding fullerene complexes by only 10–40 kJ $mol^{-1}$. Moreover the bonding energy of the unconstrained nickel pyracylene complex is 87 kJ $mol^{-1}$ lower than that of the bent-constrained complex. This points out that the constraint process is essential also to reproduce the metal–fullerene bonding energy. The results of the geometries and bonding energies calculated for the pyracylene and fullerene complexes indicate that the constrained pyracylene is a fairly good model to study the interaction of the whole organic moiety. Indeed the geometries are reproduced within 0.02 Å and the metal–fullerene interaction is only slightly underestimated.

## Electronic structure

We have analysed the interaction between pyracylene and metal fragment $M(PH_3)_2$ with the Dewar–Chatt–Duncanson model.[21] According to this model, the bond is described in terms of the electron donation from a filled π orbital of the ligand to a suitable vacant metal orbital (σ donation), and of the simultaneous back-donation from an occupied metal d orbital to the vacant π* orbital of the ligand (π back-donation). Although the physical meaning of one-electron orbitals in DFT has been debated for many years, nowadays the correspondence of Khon–Sham orbitals with respect to Hartree–Fock orbitals in the study of chemical bonding has been well established.[22–24]

The main valence orbitals of $M(PH_3)_2$ metal fragments have been discussed in detail when dealing with the transition metal complexes of $C_{60}$ (see ref. 8). The molecular orbitals of pyracylene are reported in Fig. 3 for both the planar and bent-constrained geometries. The frontier orbitals of planar pyracylene have been discussed in terms of the interaction between the two non-bonding orbitals of the [12]annulene and the π orbitals of the central bridging $C_2$ group. The HOMO $2b_{3g}$ and the second LUMO $3b_{3g}$ are respectively the in-phase and the anti-phase combination of one of the 12-π perimeter orbitals and the π* orbital of the bridging group, while the LUMO, $2b_{2g}$, is the second 12-π perimeter orbital, see Scheme 2. As a consequence of the above mixing, the HOMO $2b_{3g}$ has a small π* character on the [6,6] C–C bond, while the second LUMO $3b_{3g}$ has a strong π* character on this bond and negligible contributions on the cyclopentadiene atoms of the

**Table 3** Calculated bond dissociation energies for the $(PH_3)_2M(C_{14}H_8)$ and $(PH_3)_2M(C_{60})$ complexes (kJ mol$^{-1}$). Values calculated with basis set II are shown in parentheses

| | $E^*$ | BSSE | $E^a$ | $E^R_{M(PH_3)_2}$ | $E^R_{Ligand}$ | $D$ |
|---|---|---|---|---|---|---|
| $(PH_3)_2Ni(C_{14}H_8)$ | 202 | −29 | 173 | −42 | −8 | 123 |
| | (176) | (−8) | (168) | (−42) | (−9) | (117) |
| $(PH_3)_2Pd(C_{14}H_8)$ | 114 | −32 | 82 | −32 | −7 | 48 |
| | (80) | (−5) | (75) | (−32) | (−1) | (42) |
| $(PH_3)_2Pt(C_{14}H_8)$ | 211 | −28 | 183 | −104 | −15 | 64 |
| | (259) | (−8) | (251) | (−126) | (−16) | (109) |
| $(PH_3)_2Ni(C_{60})$ | 255 | 34 | 222 | −47 | −44 | 130 |
| $(PH_3)_2Pd(C_{60})$ | 178 | 34 | 144 | −39 | −41 | 63 |
| $(PH_3)_2Pt(C_{60})$ | 309 | 30 | 279 | −130 | −40 | 108 |
| $(PH_3)_2Ni(C_{14}H_8)$ | 139 | −34 | 104 | −26 | −42 | 36 |
| Planar | (110) | (−8) | (102) | (−32) | (−46) | (24) |

[a] $E = E^* + BSSE$.

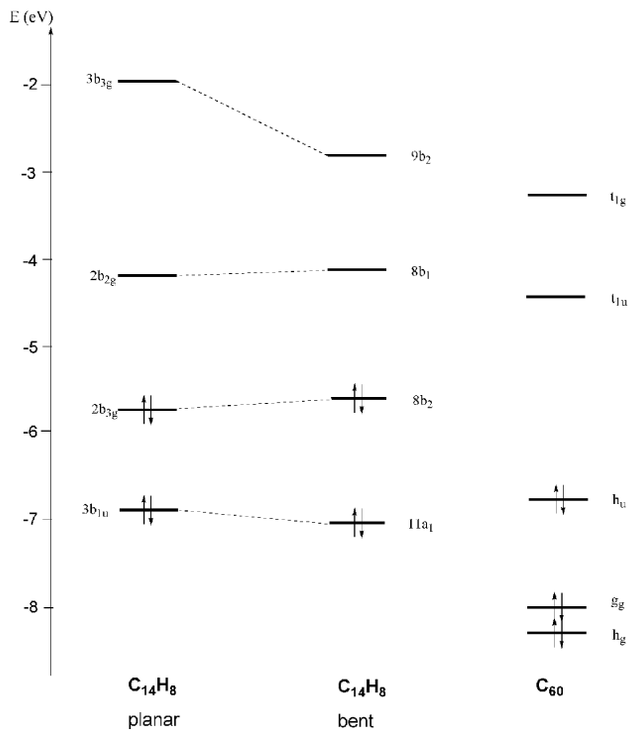


**Fig. 3** Main valence orbitals of planar and bent pyracylene compared to those of $C_{60}$.

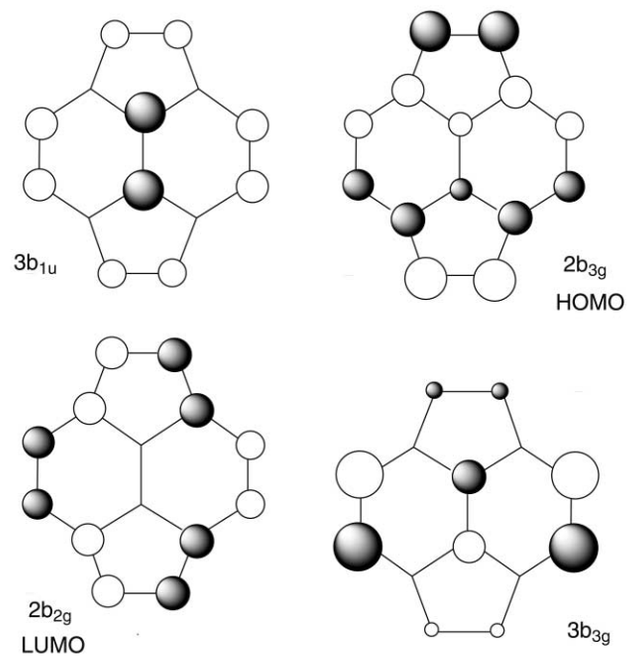


**Scheme 2**

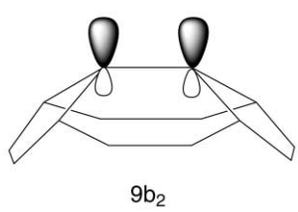


**Scheme 3**

perimeter (see Scheme 2). The second HOMO, $3b_{1u}$, on the other hand has a predominant π character on the central $C_2$ group (see Scheme 2). As result of pyracylene bending, we observe a slight destabilisation of these orbitals, except for the ones with a strong π or π* character on the $C_2$ group: the second HOMO, which is slightly stabilised, and the second LUMO, which is strongly stabilised by 0.7 eV. Moreover the π* component on the $C_2$ unit of this orbital, $9b_2$ in the $C_{2v}$ symmetry group of the bent pyracylene, mixes with the in-plane s, $p_x$ and $p_y$ orbitals of the perimeter carbon atoms, thus undergoing a polarisation towards the convex face, see Scheme 3. Fig. 3 compares also the $C_{60}$ frontier orbitals of $C_{60}$ with those of pyracylene. It is evident that the stabilisation of the second LUMO of pyracylene due to the process of bending leads the $9b_2$ orbital closer to the vacant orbitals of $C_{60}$ with π* character on the [6,6] bond. Moreover the second HOMO of pyracylene, with strong π character, is close in energy to the HOMO of $C_{60}$, which contains several components with π character on the [6,6] bond.

Fig. 4 shows the major interactions between the frontier MOs of $C_{14}H_8$ and those of the $Pt(PH_3)_2$ fragment. The electron donation into the empty metal σ orbital involves the pyracylene $11a_1$ orbital with π character at the [6,6] bond. The π back-donation from the filled metal $d_\pi$ orbital is directed essentially to the second LUMO of pyracylene $9b_2$ with π* character at the [6,6] bond. It is worth noting that the HOMO of pyracylene, which has also a partial π* character, is involved in this interaction and thus stabilised.

A Mulliken population analysis in terms of the molecular orbitals of the $C_{14}H_8$ and $M(PH_3)_2$ fragments allows the identification of the orbitals of $C_{14}H_8$ involved in σ donation and π back-donation. The results of such analysis are reported in Table 4 and show that pyracylene to metal electron donation takes place mainly from the $11a_1$ orbital of $C_{14}H_8$ to the $6a_1$ orbital (LUMO) of the metal fragment. On the other hand the back-donation from the metal fragment to $C_{14}H_8$ takes place from the metal $4b_2$ ($d_{yz}$) orbital to the $9b_2$ orbital of pyracylene.

**Table 4** Mulliken population of the $(PH_3)_2M(C_{14}H_8)$ complexes over the orbitals of the $M(PH_3)_2$ and $C_{14}H_8$ fragments

| | $M(PH_3)_2$ | | | | $C_{14}H_8$ | | |
|---|---|---|---|---|---|---|---|
| | $4a_1$ | $5a_1$ | $6a_1$ | $4b_2$ | $11a_1$ | $8b_2$ | $9b_2$ |
| Ni | 1.95 | 1.97 | 0.14 | 1.44 | 1.84 | 1.97 | 0.50 |
| Pd | 1.90 | 1.99 | −0.05 | 1.55 | 1.91 | 1.99 | 0.38 |
| Pt | 1.89 | 2.00 | 0.19 | 1.36 | 1.79 | 1.97 | 0.57 |

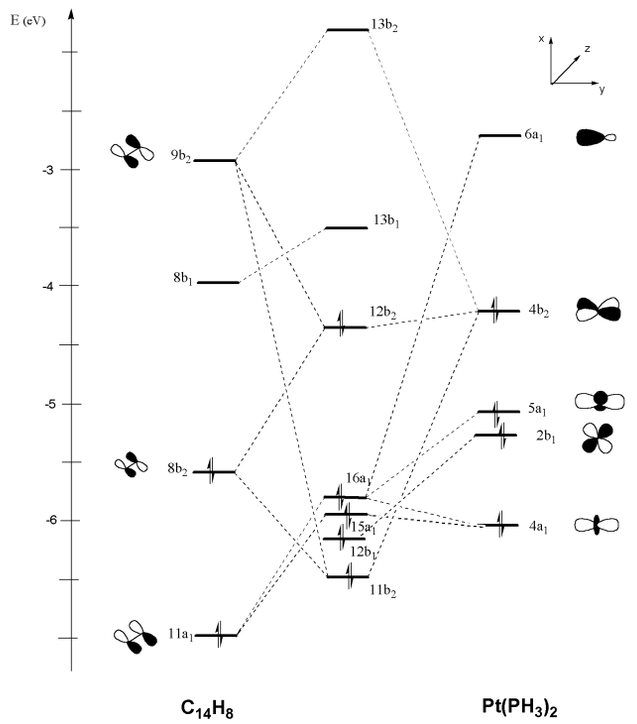


**Fig. 4** MO correlation diagram for $(PH_3)_2Pt(\eta^2\text{-}C_{14}H_8)$.

In Table 5 we have also compared the Mulliken population analysis of pyracylene and fullerene complexes. Since for both complexes we have several orbitals with the same symmetry involved both in the σ and π interaction, we made a sum of orbital depopulations of filled $a_1$ orbitals and a sum of orbital populations of empty $b_2$ orbitals for the ligand. As we can see, the overall σ donation and π back-donation are quite similar in pyracylene and fullerene complexes.

In order to separate the contributions from σ donation and π back-donation, we employed an analysis of the metal–ligand bond dissociation energy based on the extended transition state method.[25a] The bond dissociation energy is decomposed into a number of contributions:

$$D(M\text{–}C_{14}H_8) = -[E_{prep} + E_{ster} + E_{orb}] \qquad (2)$$

The first term, $E_{prep}$, is the energy necessary to convert the fragments from their equilibrium geometries to the conformation they assume in the optimised structure of the overall complex and thus corresponds to the sum of the fragments relaxation energies, $E^{R}_{C_{14}H_8} + E^{R}_{M(PH_3)_2}$. $E_{ster}$ represents the steric repulsion between the two fragments and consists of two components. The first is the electrostatic interaction of the nuclear charges and the unmodified electronic charge density of one fragment with those of the other fragment. The second component is the so-called Pauli repulsion, which is essentially due to the antisymmetry requirement on the total wavefunction. $E_{orb}$, known as the orbital interaction term, represents the attracting orbital interactions which give rise to the energy

**Table 5** Mulliken population of the $(PH_3)_2M(C_{14}H_8)$ and $(PH_3)_2M(C_{60})$ complexes

| | $M(PH_3)_2$ | | Ligand[a] | |
|---|---|---|---|---|
| Molecule | $6a_1$ | $4b_2$ | $a_1$ | $b_2$ |
| $(PH_3)_2Ni(C_{14}H_8)$ | 0.14 | 0.56 | 0.16 | 0.50 |
| $(PH_3)_2Pd(C_{14}H_8)$ | −0.05 | 0.45 | 0.09 | 0.38 |
| $(PH_3)_2Pt(C_{14}H_8)$ | 0.19 | 0.64 | 0.21 | 0.57 |
| $(PH_3)_2Ni(C_{60})$ | 0.12 | 0.69 | 0.13 | 0.55 |
| $(PH_3)_2Pd(C_{60})$ | −0.09 | 0.61 | 0.07 | 0.45 |
| $(PH_3)_2Pt(C_{60})$ | 0.16 | 0.81 | 0.21 | 0.64 |

[a] Sum of orbital depopulation of filled $a_1$ orbitals and of orbital population of empty $b_2$ orbitals of the organic ligand.

lowering upon coordination. This term may be broken up into contributions from the orbital interactions within the various irreducible representations $\Gamma$ of the overall symmetry group of the system, according to the decomposition scheme proposed by Ziegler.[25b]

This decomposition scheme is particularly useful in the considered complexes, as it allows one to separate the energy contributions corresponding to σ donation ($E_{A1}$) and to π back-donation ($E_{B2}$). Indeed, the ligand to metal donation takes place into the $A_1$ representation, while the metal to ligand back-donation takes place into the $B_2$ representation. The results of this energy decomposition for all the considered pyracylene complexes are reported in Table 6 and compared with those of fullerene complexes. It is clear that, as in fullerene complexes, the contribution to the orbital interaction term from π back-donation dominates over that from σ donation. The orbital interaction terms of the pyracylene complexes are 40–80 kJ $mol^{-1}$ lower than those of the corresponding fullerene complexes, this difference being entirely accounted for by the contribution from the π back-donation.

Both σ donation and π back-donation increases in the order Pd, Ni, Pt, showing the same trend calculated for the distortion of the $C_{14}H_8$ unit and indicated by the increase of the C–C bond length and the pyramidalisation angle (see Table 2). The above analysis allows also us to clarify the effects of the geometrical constraints on the metal–pyracylene interaction: as a result of bending, the second LUMO of pyracylene is lowered in energy and may better interact with the filled $d_\pi$ orbital of the metal fragment. This is confirmed by the large increase of the π back-donation contribution, 79 kJ $mol^{-1}$, to the nickel–pyracylene orbital interaction upon bending of pyracylene system.

## 4 Conclusions

The pyracylene molecule has been proposed as a model to study the interaction of transition metal complexes with fullerene. To reproduce adequately the geometric and electronic structure of fullerene, suitable geometric constraints have been imposed on the pyracylene model, enforcing the pyramidalisation angle on the two central carbon atoms to assume a value similar to that observed in $C_{60}$.

Density functional calculations on $(PH_3)_2M(C_{14}H_8)$ (M = Ni, Pd, Pt) molecules have been performed and the results have been compared with those of the corresponding fullerene complexes. The results show that constrained pyracylene is a fairly good model to reproduce the interaction of transition metals with fullerene: the geometrical parameters are reproduced within 0.02 Å and the bond dissociation energies are slightly underestimated by only 10–40 kJ $mol^{-1}$. The metal–pyracylene interaction has been analysed in terms of the Chatt–Dewar–Duncanson model and the contribution from π back-donation is found to dominate over that from σ donation, as occurs in fullerene complexes.

**Table 6** Bond dissociation energy decomposition for the $(PH_3)_2M(C_{14}H_8)$ and $(PH_3)_2M(C_{60})$ complexes (kJ $mol^{-1}$). Values calculated with basis set II are shown in parentheses

| | $E_{ster}$ | $E_{orb}$ | $E_{A1}$ | $E_{A2}$ | $E_{B1}$ | $E_{B2}$ |
|---|---|---|---|---|---|---|
| $(PH_3)_2Ni(C_{14}H_8)$ | 158 | −359 | −75 | −1 | −19 | −276 |
| | (164) | (−340) | (−70) | (−1) | (−18) | (−256) |
| $(PH_3)_2Pd(C_{14}H_8)$ | 189 | −303 | −86 | −3 | −20 | −206 |
| | (183) | (−263) | (−77) | (−2) | (−15) | (−175) |
| $(PH_3)_2Pt(C_{14}H_8)$ | 308 | −519 | −173 | −6 | −30 | −323 |
| | (372) | (−631) | (−226) | (−7) | (−33) | (−352) |
| $(PH_3)_2Ni(C_{60})$ | 178 | −433 | −80 | −3 | −23 | −347 |
| $(PH_3)_2Pd(C_{60})$ | 167 | −345 | −81 | −3 | −21 | −261 |
| $(PH_3)_2Pt(C_{60})$ | 287 | −596 | −168 | −7 | −34 | −410 |
| $(PH_3)_2Ni(C_{14}H_8)$ | 141 | −280 | −77 | −1 | −19 | −197 |
| Planar | (145) | (−256) | (−71) | (−1) | (−17) | (−171) |

The effect of the geometrical constraints on the metal–pyracylene bond has been verified analysing the $(PH_3)_2Ni(\eta^2\text{-}C_{14}H_8)$ complex without any constraints on the organic moiety. A lower distortion for the ligand and a lower binding energy (87 kJ $mol^{-1}$) have been found, indicating that the constrained bending is essential to reproduce the geometrical and bonding features of fullerene metal complexes.

## Acknowledgements

Thanks are due to CNR (Progetto Finalizzato "Materiali Speciali per Tecnologie Avanzate II") for financial support.

## References

1 P. W. Rabideau and A. Sygula, *Acc. Chem. Res.*, 1996, **29**, 235.
2 R. Faust, *Angew. Chem., Int. Ed. Engl.*, 1995, **34**, 1429.
3 K. K. Baldridge and J. S. Siegel, *Theor. Chem. Acc.*, 1997, **97**, 67.
4 J. M. Schulman and R. L. Disch, *J. Comp. Chem.*, 1998, **19**, 189.
5 W. E. Barth and R. G. Lawton, *J. Am. Chem. Soc.*, 1971, **93**, 1730.
6 F. Wudl, *Acc. Chem. Res.*, 1992, **25**, 157.
7 M. Solà, J. Mestres and M. Duran, *J. Phys. Chem*, 1995, **99**, 10752.
8 F. Nunzi, A. Sgamellotti, N. Re and C. Floriani, *Organometallics*, 2000, **19**, 1628.
9 E. J. Baerends, D. E. Ellis and P. Ros, *Chem. Phys.*, 1973, **2**, 42; P. M. Boerrigter, G. Velde and E. J. Baerends, *Int. J. Quantum Chem.*, 1988, **33**, 87.
10 S. H. Vosko, L. Wilk and M. Nusair, *Can. J. Phys.*, 1980, **58**, 1200.
11 A. D. Becke, *Phys. Rev. A*, 1988, **38**, 2398.
12 J. P. Perdew, *Phys. Rev. B*, 1986, **33**, 8822.
13 T. Ziegler, V. Tshinke, E. J. Baerends, J. G. Snijders and W. Ravenek, *J. Phys. Chem.*, 1989, **93**, 3050.
14 (*a*) P. M. Boerrigter, Spectroscopy and bonding of heavy element compounds, Thesis, Vrije University, 1987; (*b*) J. Li, G. Schreckenbach and T. Ziegler, *J. Am. Chem. Soc*, 1995, **117**, 486 and references therein.
15 B. M. Trost, G. M. Bright, C. Frihart and D. Brittelli, *J. Am. Chem. Soc.*, 1971, **93**, 737.
16 B. Freiermuth, S. Gerber, A. Riesen, J. Wirz and E. M. Zehnder, *J. Am. Chem. Soc.*, 1990, **112**, 738.
17 (*a*) D. A. Krovat, F. Trammell, K. E. Gilbert, J. Mitchell, J. Clardy and W. T. Borden, *J. Am. Chem. Soc.*, 1987, **109**, 5524; (*b*) W. T. Borden, *Chem. Rev.*, 1989, **89**, 1095.
18 (*a*) K. Morokuma and W. T. Borden, *J. Am. Chem. Soc.*, 1991, **113**, 1912; (*b*) J. Uddin, S. Dapprich and G. Frenking, *Organometallics*, 1999, **18**, 457.
19 S. F. Boys and F. Bernardi, *Mol. Phys.*, 1970, **19**, 553.
20 F. Nunzi, A. Sgamellotti, N. Re and C. Floriani, *J. Chem. Soc., Dalton Trans.*, 1999, 3487.
21 M. J. S. Dewar, J. A. Hashmall and N. Trinajstić, *J. Am. Chem. Soc.*, 1970, **92**, 5555.
22 F. M. Bickelhaupt, E. J. Baerends, *Kohn–Sham DFT: Predicting and Understanding Chemistry*, in *Reviews in Computational Chemistry*, eds. D. B. Boyd and K. B. Lipkowitz, Wiley-VCH, New York, 2000, vol. 15, pp. 1–86.
23 R. Stowasser and R. Hoffmann, *J. Am. Chem. Soc.*, 1999, **121**, 3414.
24 T. Kar, J. G. Ángyán and A. B. Sannigrahi, *J. Phys. Chem. A*, 2000, **104**, 9953.
25 (*a*) T. Ziegler and A. Rauk, *Theor. Chim. Acta*, 1977, **46**; (*b*) T. Ziegler, *NATO ASI, Ser. C*, 1986, **176**, 189.